Journal of Molecular Catalysis A: Chemical 305 (2009) 170–177

Contents lists available at ScienceDirect

Journal of Molecular Catalysis A: Chemical

journal homepage: www.elsevier.com/locate/molcata

Metal oxide nanowires: Preparation and application in gas sensing

Elisabetta Comini*, Guido Faglia, Matteo Ferroni, Andrea Ponzoni, Alberto Vomiero, Giorgio Sberveglieri

SENSOR Lab, CNR-INFM, Brescia University, via Valotti 9, 25133 Brescia, Italy

ARTICLE INFO

Article history:
Available online 19 January 2009

Keywords:
Nanowires
Metal oxides
Gas sensors
Heterostructures
Acetonitrile

ABSTRACT

Quasi one-dimensional nanowires of metal oxides are promising for the development of nano-devices. Sn, In, and Zn oxides were produced in form of single-crystalline nanowires through condensation from vapor phase. Furthermore longitudinal and radial heterostructures have been prepared. Nanowires growth occurs in controlled condition and allows the exploitation of size reduction effects on the electrical response to gases. Preparation, microstructural, morphological and electrical characterizations of nanowires are presented and the peculiarities of these innovative structures are highlighted.

1. Introduction

One-dimensional metal oxide semiconductor (MOX) nanowires, are interesting components for bottom-up fabrication of nanoscaled devices.

One-dimensional semiconducting nanostructures have extensive applications in sensors [1–4] optoelectronics [5], electronics, and photonics [6–11].

Nanowires bundles of metal oxides have been recently investigated for application in dye sensitized solar cells (DSC), due to their low electrical resistivity with respect to polycrystalline networks like TiO_2 nanograins presently applied in Graetzel cells [12,13].

Thanks to their intrinsic dimensions (diameters of 20–100 nm and lengths of a few micrometers) the devices produced can be very small, may have improved performance, extremely reduced power consumption that makes them appealing for applications in biological devices, nanorobotics, security monitoring, and defense technology.

The gas-sensing field for example has been extremely reassessed by the advent of quasi one-dimensional nanostructures. Quasi-1D semiconducting metal oxides, carbon nanotubes, and nano porous materials have been used as sensing elements for the preparation of conductometric sensors. They have several properties attractive for chemical sensing application: their high surface to bulk ratio; most of the atoms are available for surface reactions with surrounding molecules. The Debye length (a measure of the electronic 'cross-talk' between the surface processes and bulk electronic structure) is comparable to their lateral dimension therefore electronic properties are strongly influenced by surface processes. Moreover, nowadays fine control over the faceting, morphology, composition, doping level, defined stoichiometry and high crystallinity can be achieved. On the contrary in traditional polycrystalline gas sensors, the high temperature required for the surface reactions to take place induces a grain growth by coalescence and prevents the achievement of very stable materials. The required anisotropic growth can be obtained in different conditions, due to the crystallographic structure of the substrate, to the confinement obtained by a template, controlling other growth parameters. We have focused our research to the technique used for the preparation of most of single-crystalline gas sensor, i.e. bottom up processes.

This work presents the preparation of Sn and In oxide nanostructures focusing on their exploitation for nanoelectronic applications. A methodology to prepare hetero structures and conductometric gas sensors is presented. The functional tests have been focused on the conductometric devices for acetonitrile (C_2H_3N) sensing. The importance of detecting acetonitrile (in the following shorted as ACN) is strongly due to warfare applications, where it is used as simulant for cyanide compounds during the development of cyanide detectors [14,15]. Few works have been published yet concerning the use of metal oxide based gas sensors to detect similar gases, most of them focused on tin oxide layers prepared by thin or thick film technologies. These works showed the suitability of such materials to detect ACN at ppm concentrations, but further work is necessary to exploit the contribution hat these materials could give to the field, especially using nanowires based devices, which open the prospective of achieving improved sensitivity and stability.

2. Experimental

2.1. Preparation procedure

Metal oxide nano-crystals have been prepared according to the recently proposed evaporation–condensation process, with

* Corresponding author.
E-mail address: comini@sensor.ing.unibs.it (E. Comini).

1381-1169/$ – see front matter © 2009 Elsevier B.V. All rights reserved.
doi:10.1016/j.molcata.2009.01.009

Vapour–Solid (VS) and Vapour–Liquid–Solid (VLS) growth mechanism. Such a deposition technique consists of thermally driven evaporation of bulk metal oxides followed by condensation.

The materials studied were In oxide and Sn oxide. The experimental set-up for the oxide deposition consists of a high temperature alumina furnace capable to activate decomposition of the oxide precursors and to promote evaporation. The evaporation temperature was 1500 °C and 1370 °C for In oxide and Sn oxide, respectively. The controlled pressure of the inert atmosphere and the gradient of temperature within the furnace allow condensation and nucleation of the nanostructures downstream the inert Ar gas flow. The pressure was in the range 50–200 mbar and the flux in the range 50–200 standard cubic centimetres per minute (sccm). These peculiar non-equilibrium conditions promote formation of nanosized 1D structures. The pressure, the temperature gradient and the carrier flux have to be strictly controlled in order to guarantee the reproducibility of the deposition process. Catalyzed and catalyst-free growth was exploited, in order to investigate the influence of the catalysts on the shape and dimensions of the nanowires and on the consequent modification of their functional properties. To prevent the nanowires from contamination, two deposition systems were separately used.

The noble metal catalysts such as In, Pd, Pt and Au were deposited by sputtering on the substrate. In order to have cluster formation and not a continuous film we have reduced the deposition time and the applied power to the target, 20 W and 1 s, 50 W and 2 s, 50 W and 10 s, 50 W and 5 s, respectively. The ability to control the size and dispersion of the catalyser is fundamental since it allows in turn the control of the size and dispersion of nanowires.

Au nanoparticles with a well-defined cluster dimension dispersed in a colloidal solution (BBInternational) were also used as catalysts.

Indium and tin oxide nanowires have been produced using different catalysts over different substrates. In, Au and Pt were applied for substrate seeding before condensation for indium oxide nanowires preparation. While Pt, Au, Sn and Pd were used for tin oxide nanowires preparation. Polycrystalline Al_2O_3, a-plane sapphire, silicon and silicon carbide substrates were used. Different growth mechanisms were involved depending on the catalyst and the substrate.

2.2. Electron microscope

Scanning and transmission electron microscopy (SEM and TEM) have been carried out in order to determine the degree of homogeneity and crystalline arrangement.

The as-prepared structures were observed at low accelerating voltage, in order to avoid the electrostatic charging of the insulating substrate. The optimal voltage for observation of un-prepared specimens was found to be in the 2–3 keV range.

The nanostructures have been removed from the substrate used for deposition through dry scratching with a razor blade and dropped over a standard holey carbon film grid. Standard removal trough sonication in alcohol has been avoided to prevent the thin structures from breaking. The thin substrate was used for both conventional TEM observation and Energy Dispersive X-ray Spectroscopy (EDX) analysis at the SEM with improved spatial resolution. In addition, the conductive carbon film allowed one to increase the beam voltage up to 20 keV for effective generation of the characteristics X-rays from the specimen.

High-resolution TEM imaging is useful for investigation of the termination of the nanowire lateral sides and apex. Electron diffraction (ED) and analysis of zero-order and higher order Laue-zones allows precise determination of unit cell and space group.

The nano-manipulation set-up for in-situ electrical measurement was implemented in a LEO 1525 FEG SEM operated at the 3–5 keV accelerating voltage range. The manipulation system was based on two Kleindiek piezo-actuated probes, capable of sub nanometric positioning resolution, and a Keithley mod 6487 picoammeter/voltage source.

2.3. Atomic force microscope

The morphology has been investigated by means of Atomic Force Microscopy (AFM). Measurements have been carried out in air with a Thermomicroscope-Veeco CP-Research working in tapping mode with high-resolution silicon tip (Nanosensors, SSS-NCHR model). The sharp tip termination (nominal radius value is 2 nm) together with its high aspect ratio [16] reduce the tip-sample convolution effects that can alter the proper imaging of structures characterized by sharp height-steps such as nanowires and nanobelts.

Since these nanostructures grow perpendicularly to the substrate and cannot be easily measured as grown by AFM, they have been transferred over a flat Si/SiO_2 substrate by slightly frictioning the two substrates (Si/SiO_2 and alumina) together, obtaining dispersed nanostructures horizontally laying over the flat Si/SiO_2 substrate.

2.4. Functional measurements

Gas sensing tests have been carried out by flow through method in a thermostatic sealed chamber with controlled temperature and humidity. Dry air certified bottles and permeation tubes have been used as gas source [17] and certified mass flow controllers to reproduce desired gaseous composition inside the test chamber. A detailed description of the setup is reported in [18].

All measurements have been carried out at a constant flow of 0.3 Standard Litre per Minute (slm), constant humidity and chamber temperature (RH = 30% @ 20 °C).

3. Results and discussion

3.1. Indium oxide

Application of In thin layer over polycrystalline alumina (Fig. 1, top) resulted in formation of In_2O_3 nanograins during the preliminary heating of the furnace, and consequent nanowires nucleation and growth according to the direct vapor solid (VS) mechanism [19]. Each nanowire nucleates from an In_2O_3 nanograin, as clearly visible in the inset of Fig. 1, top, which illustrates the early condensation stage of the process. Prolonged condensation results in formation of a nanowires bundle. Au and Pt, instead, do not interact with oxygen during the transient heating, and act as liquid catalyst during the condensation step. They are able to capture the volatiles transported by the Ar flux, forming a eutectic alloy. Precipitation of In occurs when the supersaturation is reached, and the nanowire originates from the liquid catalytic tip, which indefinitely remains at the apex of the nanowire (vapor–liquid–solid (VLS) growth mechanism) [20]. Depending on the substrate, the nanowire can grow either randomly oriented, in case of polycrystalline substrate (Fig. 1, center), or along preferential direction. In case of a-sapphire substrate, good matching exists between the lattice of the substrate (lattice constant $a = 0.476$ nm) and of the In_2O_3 nanowires ($a = 1.01$ nm), inducing perfect alignment of most nanowires to the direction normal to the substrate surface (Fig. 1, bottom).

3.2. Tin oxide

Concerning tin oxide nanostructures Fig. 2 reports the summary of the morphologies obtained for each catalyst at different deposition temperatures using alumina substrates. The use of Pt catalyst

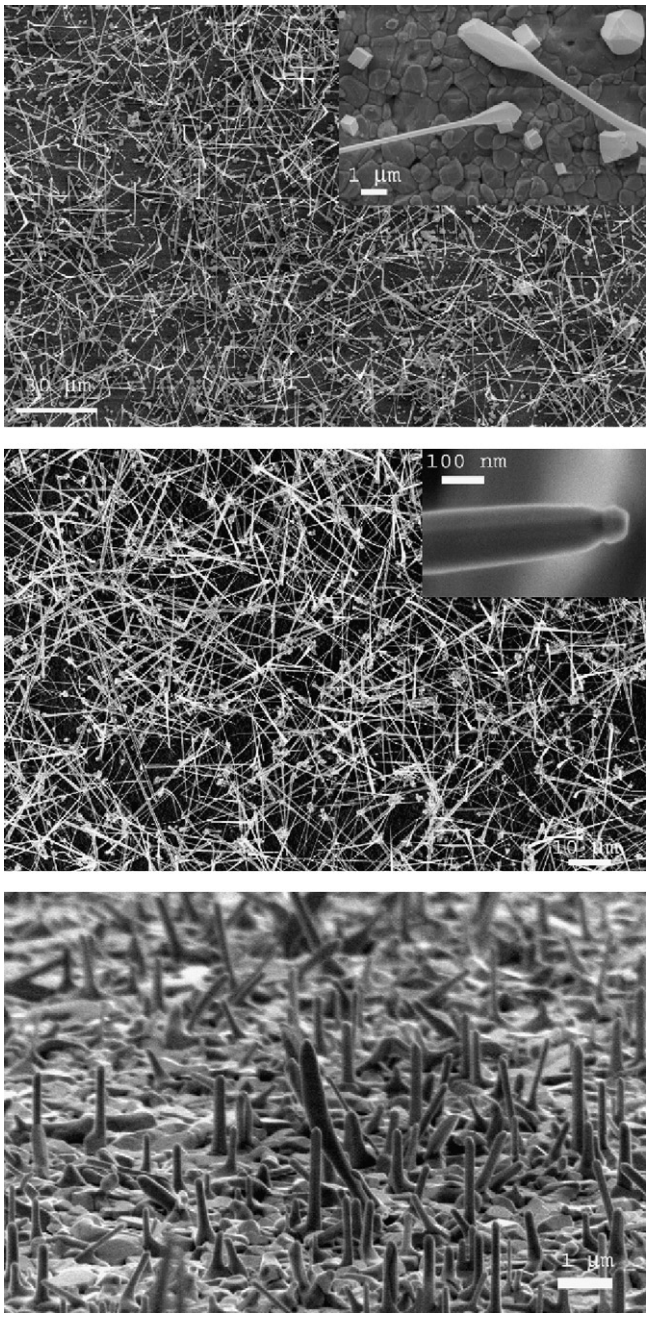

Fig. 1. Top: self catalyzed In_2O_3 nanowires. Top inset: early nucleation stage of the nanowires from In_2O_3 seeds formed over the polycrystalline alumina substrate after short-time condensation. Center: heterocatalysis of In_2O_3 nanowires growth using Pt thin layer. During furnace heating Pt droplets are forming, which lead nanowires growth according to the VLS mechanism. Center inset: magnified picture of a metallic tip of a nanowire. Bottom: oriented growth of In_2O_3 nanowires over a-sapphire substrate (tilted view: $\theta = 45^\circ$). Small Au droplets are applied as external catalysts. The combined action of Au catalyst and of the single crystal substrate force the VLS growth of the nanowires parallel to the direction normal to the substrate surface.

lead to the nanowires formation in a wider range of temperatures compared to the other catalysts. Sn and Pd catalysts instead form microwires and 3D structures. As in the case of In oxide described before, Sn particles oxidize and form seed for the nanowires growth, while the other catalysts act as liquid catalyst during the condensation step.

Fig. 3 shows a SEM image of Sn oxide nanowires deposited with Pt catalyst, while Fig. 4 reports the microwires formation in the case of Sn catalyst. The two samples appear similar in morphology as

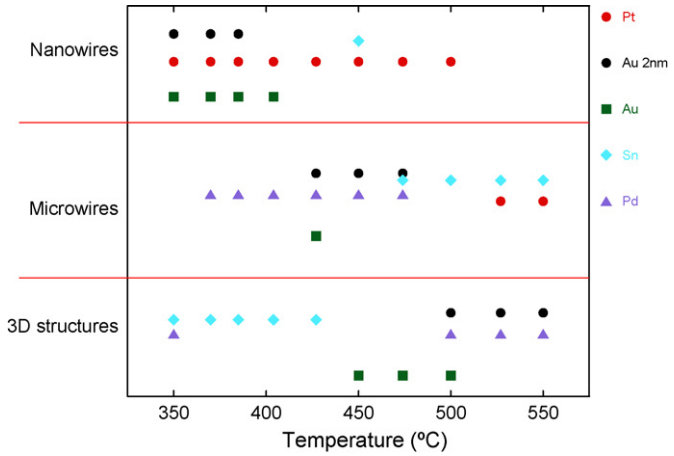

Fig. 2. Summary of the SnO_2 morphologies obtained for different catalysts and deposition temperatures.

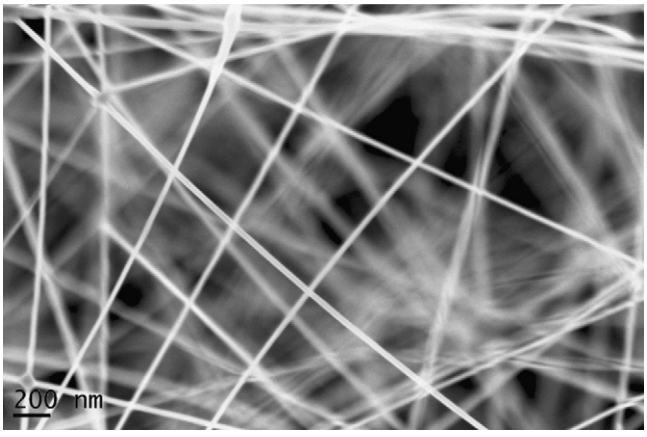

Fig. 3. Sn oxide nanowires deposited with Pt catalyst at a deposition temperature of 390 °C.

dense bundles of long structures have been obtained. However, the large difference in lateral size and length for the two samples should be noticed. The microwires shown in Fig. 4 maintain the uniform section and constant width as it was achieved for the nanowires in Fig. 3. Fig. 5 shows the catalytic tip at the top of the nanowires obtained with Au catalyst, an evidence of the catalytic growth.

Within the detection limit of EDX microanalysis, the nanostructures of indium and tin oxide resulted free from contaminating

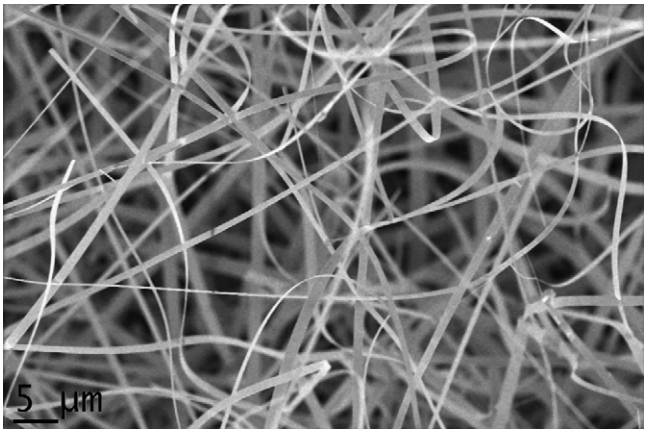

Fig. 4. Sn oxide microwires deposited with Sn catalyst at a deposition temperature of 480 °C.

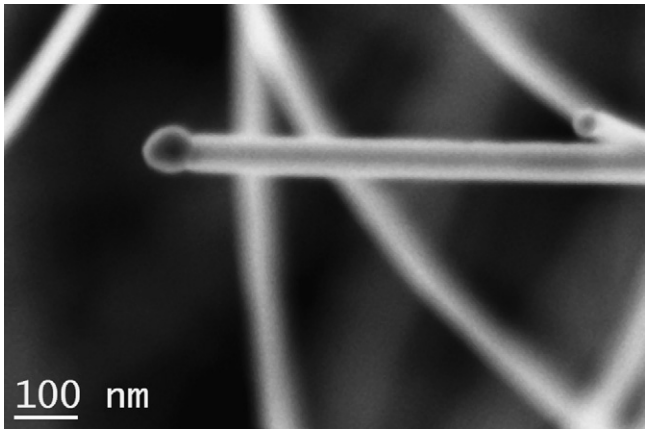

Fig. 5. Sn oxide nanowires deposited with Au catalyst at a deposition temperature of 300 °C. The presence of the catalytic tip at its apex confirms the Au catalytic activity.

elements. This result was obtained basically though the usage of a separated deposition systems. The nanowires do not require post-synthesis annealing, a fabrication step prone to contamination, because the good crystalline quality is readily achieved though the peculiar nucleation and growth mechanism.

3.3. Heterostructures

Linear heterostructures can be created via sequential condensation of different precursors, the first having a higher sublimation temperature [21]. The heterogeneous catalyst maintains its catalytic activity during both the condensation steps, resulting in a sequential VLS–VLS process. Au metal catalyst has been used for the fabrication of the longitudinal heterostructure (Fig. 6). The growth of In_2O_3 nanowires is catalyzed by Au nanoparticles on sapphire substrate. In fact, the substrate was preliminarily seeded with Au nanoparticles. In this case In_2O_3 nanowires were produced via VLS mechanism. The Au particle at the apex of the In_2O_3 nanowire also promotes the nucleation of SnO_2 nanowire during the second condensation, leading to formation of the longitudinal heterostructure.

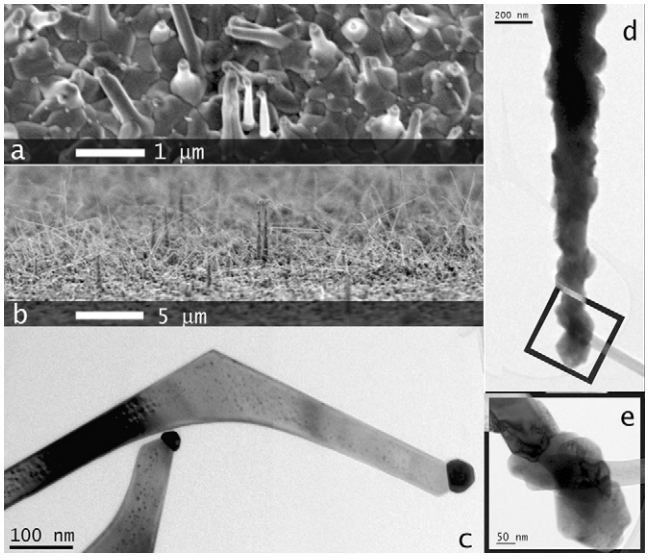

Fig. 6. Images of of In and Sn oxides. (a) In oxide nanowires fabricated by Au-catalyzed VLS growth. (b) Panoramic SEM view of Sn and In nanowire heterostructures prepared over sapphire substrate. (c) Detail of the SnO_2 nanowires with Au catalytic particle at the apex. (d) Longitudinally assembled heterostructure of In and Sn obtained by two-step Au-catalyzed VLS condensation (e) detail from the boxed area in (d) of the junction between the two nanowires.

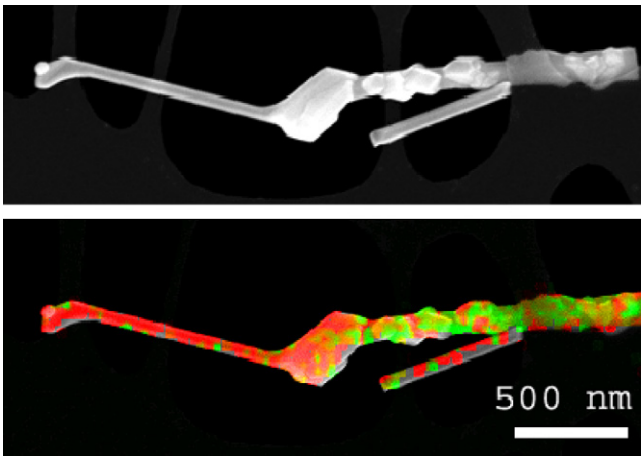

Fig. 7. (Top) SEM image of SnO_2–In_2O_3 heterostructure. (Bottom) EDS elemental distribution of Sn (red) and In (green). (For interpretation of the references to color in this figure legend, the reader is referred to the web version of the article.)

ture. In Fig. 7 a linear heterostructure is shown, composed by In_2O_3 (green signal in the EDS mapping of Fig. 7, bottom) and SnO_2 (red signal). At the apex of the SnO_2 nanowire the Au catalytic tip is clearly visible. During the growth of the SnO_2 nanowire, concurrent condensation of SnO_2 on the lateral sides of the In_2O_3 nanowire occurs, as testified by the red EDS signal and the polycrystals well visible in Fig. 7, top.

Both nanowires of In and Sn oxide preserve the crystalline arrangement ([1 0 0] and [1 0 1] growth direction for In and Sn oxide nanowires, respectively) that is commonly obtained through evaporation–condensation. Indeed, the nanowires are single crystalline, with well-shaped crystal habit, and the crystalline phase is cubic and rutile–tetragonal for In and Sn oxide, respectively.

Radial heterostructures can be also fabricated, using a two-steps process without addition of any catalyst [21]. A single-crystalline nanowire grown by direct VS condensation acts as a backbone for a second condensation step, in which polycrystalline nanograins completely cover the backbone. In these conditions no catalyst is required, which could lead to anisotropic growth of a longitudinal heterostructure.

3.4. Atomic force microscopy analysis

The Atomic Force Microscopy (AFM) analysis provides results that are complementary respect to the ones obtained by SEM measurements. The cross-section of the grown nanostructure can be easily determined by AFM, thus enabling the distinction between nanostructures grown with belt- or wire-like morphology.

As case study, AFM measurements have been carried out on tin oxide nanostructures dispersed over the flat Si/SiO_2 substrate, observing the presence of both nanobelts and nanowires morphologies. The three dimensional image of a wire-like nanostructure is shown in Fig. 8a).

Six nanostructures have been imaged by AFM and results are summarized in Fig. 8b) by means of the measured height (h) and full width at half maximum (FWHM).

Despite the high-resolution tip used for AFM measurements reduces the tip-sample convolution effects, they cannot be avoided at experimental level and they manifest mainly in FWHM estimation. To account for this effect, the FWHM error has been calculated based on the guaranteed tip features.

Based on such measurements, only one nanostructure among the six imaged exhibit wire morphology (h/FWMH = 1.2) while the other five exhibit belt like morphology with the h/FWHM ratio ranging from 2 to 9.

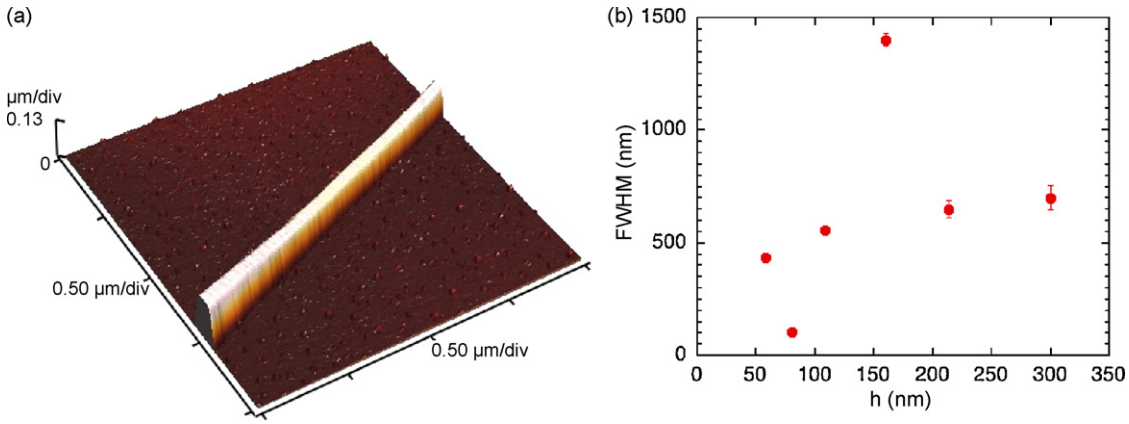

Fig. 8. Three-dimensional AFM image of a single SnO_2 nanostructure exhibiting wire-like shape dispersed over a Si/SiO_2 substrate (a). Height (h) and full width at half maximum (FWHM) characterization of 6 nanostructures (b). The FWHM uncertainty has been calculated according to the tip specifications (guaranteed aspect ratio and tip angle).

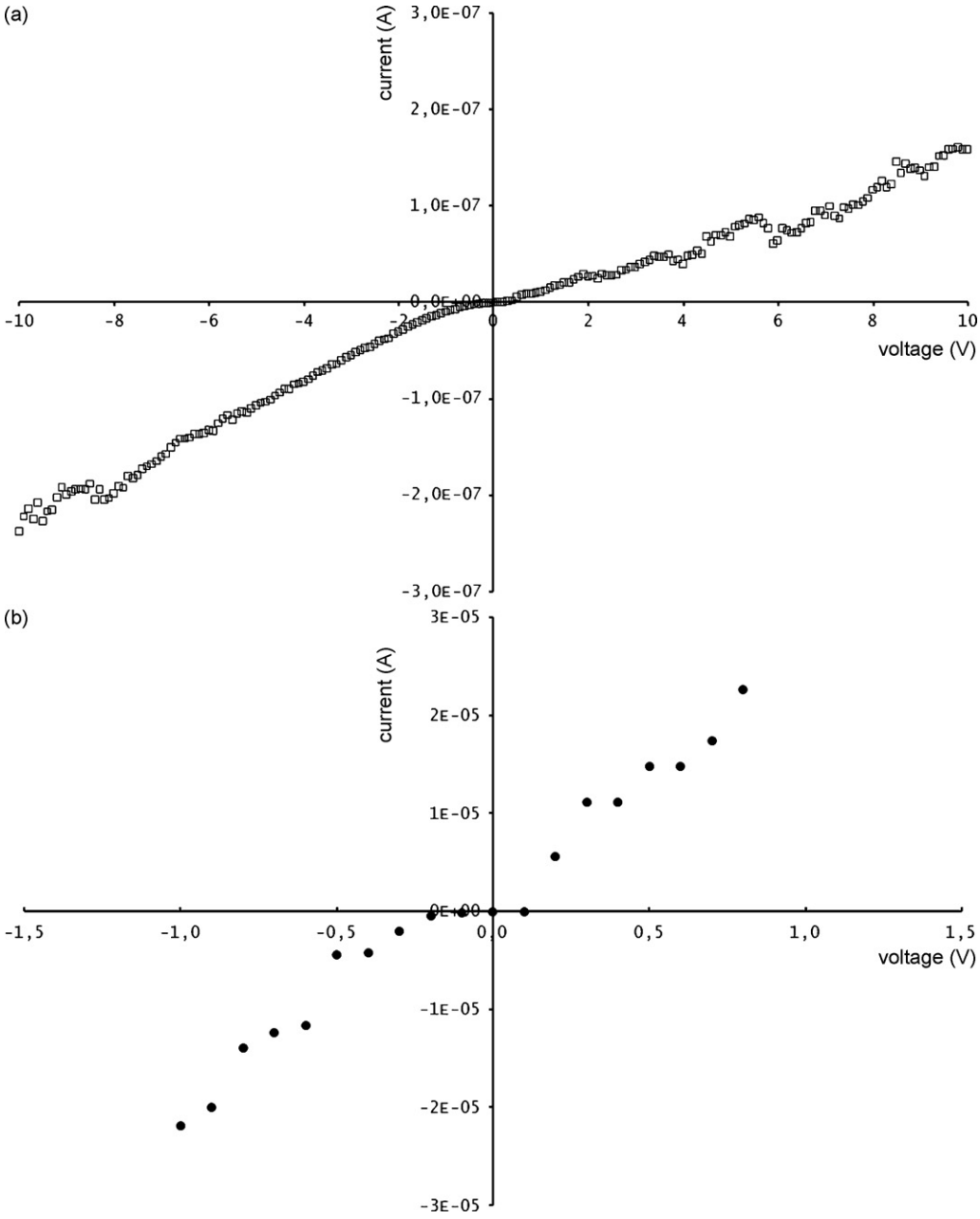

Fig. 9. Current–voltage plot of SnO_2 and In_2O_3 nanowires as measured by two-probe manipulation set-up.

3.5. Electrical characterization

The electrical characterization of nanowire-like structures through manipulation techniques has been developed with the purpose to measure the transport properties of single nanowires without integration of the growth into a functional substrate [22]. The methodology for manipulation of nanowires has largely benefited from the previous efforts expended for the characterization of carbon nanotubes and nanostructures [23,24], and is carried out in association with highly resolved imaging techniques such as scanning electron microscopy (SEM) [25].

The characterization of metal oxide nanowires has been performed via a two-contacts method, where the conductive paths are provided by piezo-actuated sharp metallic probes. Fig. 9 shows the measured current–voltage characteristic of SnO_2 and In_2O_3 nanowires, the first one over a wide range of applied voltage and the second one close to the origin. The experimental evidence indicates that the electrical behavior is nearly ohmic over a wide voltage range. The curve is reproducible and the Schottky barrier between the metallic tungsten probe and the semiconducting nanowire did not affect the overall behavior.

The method was proved effective in measuring the electrical properties of longitudinally assembled nanowires of In and Sn oxides. The capability to probe the local electrical transport at the nanoscale resulted useful in evaluating the potential of heterogeneous structures [21]. Moreover, the capability to accurately locate a conducting probe with nearly spherical termination in proximity of a single nanowire allows one to perform as a complex measurement as the determination of the field emission properties.

Indeed, the nanowires are promising basic elements for the fabrication of electron emitters owing to their crystalline quality, as illustrated in [26].

3.6. Gas sensing characterization

The peculiar structural and morphological properties of metal oxide nanowires are suited features for the development of innovative devices and, in particular, gas sensors.

The sensing mechanism underling semiconducting metal oxides relies on redox reactions occurring between gaseous molecules and active ions such as OH^-, O^{2-}, O^- adsorbed over the metal oxide surface depending on its temperature [27]. Such red-ox reactions modulate the surface population of the above active ions and thus the space charge layer depth within the metal oxide.

Based on these findings, the key features conferring high sensitivity to nanowires are their nanosized transversal dimensions and the high aspect ratio [28]. The quasi one-dimensional structure confines the charge carriers on a wired-path with lateral dimensions close to the size of the space charge region (few tens of nm [29]) so that the space charge layer extends through the whole electrical wire-path and modulates the entire conducting channel.

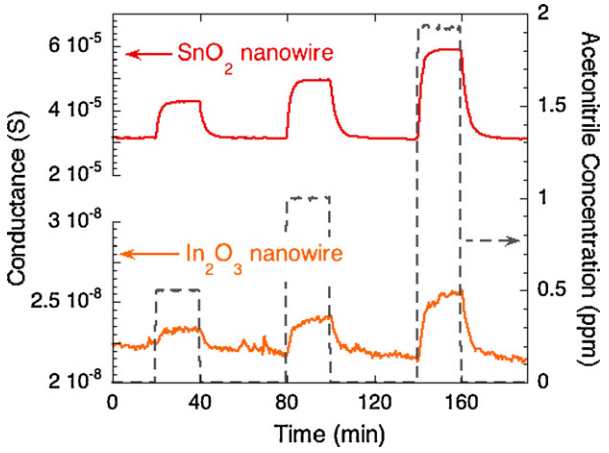

Fig. 10. Dynamic response exhibited by SnO_2 nanowires and In_2O_3 nanowires sensors heated at the temperature of 500 °C to different acetonitrile concentrations.

Gas sensing measurements have been focused on acetonitrile (ACN), used as simulant for cyanide compounds. The Immediately Dangerous for Life and Health (IDLH) value is one of the widest used parameters to quantify a compound toxicity. For cyanides compounds, the IDLH value is few tens of ppm, depending on the particular molecule [14]. Gas sensing measurements have been carried out at different acetonitrile concentrations lower than the above IDLH value, in order to obtain data useful for the development of systems suited for early detection of such compounds. Dynamic responses of SnO_2 nanowire and In_2O_3 nanowire sensors heated at the working temperature of 500 °C are shown in Fig. 10. It is evident that at such temperature, which corresponds to the best sensing conditions according to Fig. 11(a) and (b), the sensor signal of both sensors follows the acetonitrile concentration and recovers the baseline value once the analyte injection is stopped. The time required to reach steady state values both during response and recovery processes is comparable with the test chamber filling/purging time (about 180 s).

A more detailed analysis of response and recovery time is reported in Fig. 11(a) and (b) for SnO_2 and In_2O_3 nanowires sensors, respectively. In these plots, sensor responses are summarized by means of three parameters: response time (τ_{RISE}), recovery time (τ_{FALL}) and sensor response amplitude, depicting their dependence

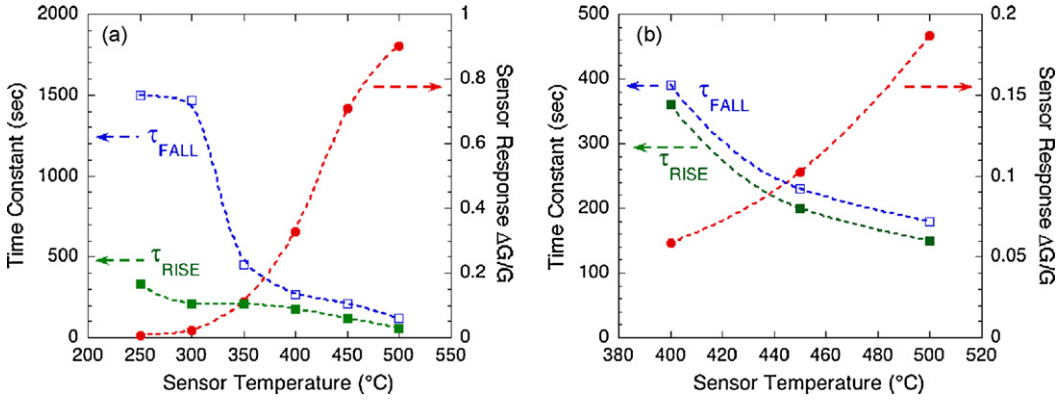

Fig. 11. Response parameters dependence from the sensor temperature calculated from the SnO_2 nanowires (a) and In_2O_3 nanowires (b) sensor response to 1.9 ppm of acetonitrile. Axes scales are different in (a) and (b) figures due to the different values obtained from SnO_2 and In_2O_3 sensors. Concerning indium oxide, data acquired at temperatures below 400 °C have not been reported because the weak response does not allow to calculate reliable response parameters.

on the sensor temperature. τ_{RISE} (τ_{FALL}) are calculated fitting by an exponential law the response (recovery) dynamics of the sensor signal after the injection of 1.9 ppm of acetonitrile is started (stopped). Response amplitude is calculated as $(G_f - G_0)/G_0$, where G_0 and G_f represent the steady state value of the sensor conductance in the reference air and reference air plus 1.9 ppm of acetonitrile.

It is evident from Fig. 10 that the SnO_2 bundle is more conductive than the In_2O_3 bundle. The electrical conductance of the device depends both on the conductivity of each nanowire but also from the network connection of the network. The electrical properties of single nanowires have been analyzed in Fig. 9, where it is evident that In_2O_3 nanowires are more conductive than SnO_2 nanowires. Concerning network properties, a quantitative analysis of the phenomena need the development of complex models and the use of ad-hoc developed device layout [30,31]; nevertheless, the SEM analysis reported in previous sections provide useful information to account for the low conductance exhibited by the indium oxide bundle. The SEM image of SnO_2 nanowires shown in Fig. 3 evidences the presence of a large amount of nanowires (some out of focus nanowires can be observed below the focused ones). Differently, the In_2O_3 bundle shown in Fig. 1 evidences a network composed by dispersed nanowires, which leave visible the underlying substrate.

It is also evident from Figs. 10 and 11, that the SnO_2 sensor is more sensitive than the In_2O_3 sensor. The former exhibits a response amplitude (Fig. 11a) that reach values as high as 0.9 (90%), the latter response does not reach 0.2 (20%) within the tested ACN concentrations (Fig. 11b).

These different performances will be useful once selectivity is concerned and addressed by the use of an electronic nose: a sensor array composed by sensors featuring different sensing capability provided with a pattern recognition software that associate the array-response to the presence of target gases in the atmosphere [32].

Beside these differences, the same temperature dependence of the response parameters is observed for both materials (Fig. 11a and b), suggesting that, at least in first approximation, similar phenomena occur with both materials.

According to literature [33], ACN can interact in different ways with metal oxides: it can behave both as a soft Lewis base interacting with surface acid sites or protonic centres and as a weak Brønsted acid interacting with oxygen ions adsorbed over the oxide surface.

In order to get insight on the reaction occurring in acetonitrile detection, it is worth to refer to the temperature dependence of active ions population over metal oxides. According to literature [27], at low temperature the most abundant ion is OH^-, whose population decreases with increasing temperature. Differently, oxygen ions exhibit the opposite trend, with population increasing with temperature and stabilizing as O_2^- and as O^-, with temperature increasing up to 400–500 °C. As the oxide temperature is raised, desorption begins to dominate over the oxygen chemisorption process and ion population decreases [27].

So far, based on the temperature dependence of the sensor response to ACN, it is reasonable to argue that the ACN-oxide interaction transduced to sensor response is based on ACN interaction with O^- ions. Other interactions that may occur in the tested temperature range (250–500 °C) are not appreciably transduced to sensor response.

Furthermore, the fast recovery time observed in our measurements indicates that such an ACN-oxide reaction is reversible, the activation energy of desorption being thermally provided. The existence of a thermally activated process is confirmed by the decrease of response and recovery time with temperature (Fig. 11).

Non-reversible adsorption in general produces very long desorption times and a non-full recovery in metal oxide based gas sensors. For example, the poisoning effects observed even at elevated temperature (500–600 °C) exposing metal oxide catalyst to dimethyl methylphosphonate (DMMP), a simulant for Sarin nerve agents, in high doses (thousands of ppm for tens hours) have been attributed to the irreversible adsorption of DMMP [34]. Similarly, the long recovery time measured for metal oxide gas sensors working at these temperatures and exposed to weak DMMP doses (few ppm or below for few tens of minutes) has been attributed to such poisoning phenomena [35,36]. Similar behavior has been confirmed to occur after exposure to Sarin molecules [35].

A further confirmation of the direct role of O^- ions comes from the sensor conductance increase occurring with acetonitrile exposure (Fig. 10). The reversibility of the reaction means that reaction products do not remain bonded over the oxide surface but desorbs as gaseous species. Involving O^- ions means that they bond to ACN and/or its decomposition products, thus releasing back in the oxide conduction band the electric charge previously extracted during the chemisorption process.

Compared with results reported in literature on thin and thick films, nanowires exhibit similar response amplitude (at least focusing on SnO_2, for which literature data are available), but optimal performances are obtained at higher temperature: 500 °C instead of 350–400 °C [15]. This is sometimes regarded as a disadvantage because of the higher power supply required. Nevertheless, power supply can be strongly lowered by integration of metal oxides with micromachined hotplates, which can reach temperatures as high as 500 °C by supplying few mWatts [37]. Differently, gaining optimal response amplitude at higher temperatures means lower response and recovery times (Fig. 11a and b), suited for fast-detection purposes. Furthermore, looking at the real scenario where these sensors may be used, the presence of poisoning gases such as Sarin may also be foreseen; yet the high working temperature is reported as a suited solution to reduce poisoning effects induced by such compounds [34–37].

4. Conclusions

In the last year a great effort has been put into understanding and controlling the growth process for the preparation of high quality quasi one-dimensional nanostructures. We have shown how controlled oxide nanostructures and hetero-structures can be prepared by the use of the vapor phase technique. Furthermore we have made a systematic study on how the catalyst can influence the morphology of the obtained nanostructures.

These nanostructures are interesting for different applications. Concerning gas sensing application MOX NWs demonstrate high sensitivity to various gases. In this work we have chosen the case study of acetonitrile, which is interesting for warfare applications.

The functional tests performed show interesting results for the detection of ACN with a detection limit below ppm levels and relatively fast response and recovery times.

Greater surface to volume ratio, better stoichiometry and greater crystallinity degree compared to polycrystalline oxides reduce instability and make these materials very promising for the development of a new generation of sensors. Selectivity still remains a concern. Possible ways to improve NWs selectivity may be surface coating with chemical selective membrane, modification by functional groups, or combining multi-component sensing modules coupled with signal processing functions, acting as an “electronic nose” to discriminate gas concentrations in a complex environment.

Acknowledgements

This work was partially supported, within the EU FP6, by the ERANET project “NanoSci-ERA: NanoScience in the European Research Area”.

This work was supported by the European Strep project no. 001528 "Nano-structured solid-state gas sensors with superior performance" (NANOS4), by the NATO project no. 982166 "Chemical threat detectors based on multisensor arrays and selective porous concentrators" and by INFM Seed Project 2008.

References

[1] Y. Cui, Q. Wei, H. Park, C.M. Lieber, Science 293 (2001) 1289.
[2] F. Patolsky, B.P. Timko, G. Yu, Y. Fang, A.B. Greytak, G. Zheng, C.M. Lieber, Science 313 (2006) 1100.
[3] X.D. Wang, J. Zhou, J.H. Song, J. Liu, N.S. Xu, Z.L. Wang, Nano Lett. 6 (2006) 2768.
[4] L. Senesac, T.G. Thundat, Mater. Today 11 (2008) 28.
[5] X.F. Duan, Y. Huang, R. Agarwal, C.M. Lieber, Nature 421 (2003) 241.
[6] M.S. Gudiksen, L.J. Lauhon, J. Wang, D.C. Smith, C.M. Lieber, Nature 415 (2002) 617.
[7] S.J. Tans, A.R.M. Verschueren, C. Dekker, Nature 393 (1998) 49.
[8] A. Bachtold, P. Hadley, T. Nakanishi, C. Dekker, Science 294 (2001) 1317.
[9] A. Javey, J. Guo, Q. Wang, M. Lundstrom, H.J. Dai, Nature 424 (2003) 654.
[10] M. Huang, S. Mao, H. Feick, H. Yan, Y. Wu, H. Kind, E. Weber, R. Russo, P. Yang, Science 292 (2001) 1897.
[11] C. Fasth, A. Fuhrer, L. Samuelson, V.N. Golovach, D. Loss, Phys. Rev. Lett. 98 (2007) 266801.
[12] J.B. Baxter, E.S. Aydil, Appl. Phys. Lett. 86 (2005) 053114.
[13] M. Law, L.E. Greene, J.C. Johnson, R. Saykally, P. Yang, Nat. Mater. 4 (2005) 455–459.
[14] M. Utriainen, The 11th International Meeting on Chemical Sensors, July 2006, Brescia, Italy, 2006, pp. 136–137.
[15] N.J. Choi, J.H. Kwak, Y.T. Lim, T.H. Bahn, K.Y. Yun, J.C. Kim, J.S. Huh, D.D. Lee, Sens. Actuator B-Chem. 108 (2005) 298–304.
[16] http://www.nanosensors.com/SSS-NCHR.htm.
[17] J.J. McKinley, R.E. Majors, LC-GC 10 (2000) 1024–1033.
[18] H.E. Endres, H.D. Jander, W. Gottler, Sens. Actuator B-Chem. (1995) 163–172.
[19] A. Vomiero, S. Bianchi, E. Comini, G. Faglia, M. Ferroni, G. Sberveglieri, Cryst. Growth Des. 7 (2007) 2500–2504.
[20] G. Cao, Nanostructures & Nanomaterials, Imperial College Press, London, 2004.
[21] A. Vomiero, M. Ferroni, E. Comini, G. Faglia, G. Sberveglieri, Nano Lett 7 (2007) 3553–3558.
[22] F. Hernandez-Ramirez, A. Tarancon, O. Casals, E. Pellicer, J. Rodriguez, A. Romano-Rodriguez, J.R. Morante, B. Barth, S. Mathur, Phys. Rev. B 76 (2007) 085429.
[23] M.F. Yu, O. Lourie, M.J. Dyer, K. Moloni, T.F. Kelly, R.S. Ruoff, Science 287 (2002) 637–640.
[24] A.S. Walton, C.S. Allen, K. Critchley, Ł.M. G'orzny, J.E. McKendry, R.M.D. Brydson, B.J. Hickey, S.D. Evans, Nanotech 18 (2007) 065204.
[25] Z.L. Wang, Adv. Mater. 15 (2003) 1497–1514.
[26] J. Zhou, N.S. Xu, S.Z. Deng, J. Chen, J.C. She, Z.L. Wang, Adv. Mater. 15 (2003) 1835–1840.
[27] P.T. Moseley, J. Norris, J.O.W. Norris, D.E. Williams, Techniques and Mechanisms in Gas Sensing, Adam Hilger, Bristol, 1991, Chapter 2 and 3.
[28] E. Comini, Anal. Chim. Acta 568 (2006) 28–40.
[29] N. Barsan, U. Weimar, J. Electroceram. 7 (2001) 143–167.
[30] D.J. Frank, C.J. Lobb, Phys. Rev. B 37 (1) (1998) 302–307.
[31] E.S. Snow, J.P. Novak, P.M. Campbell, D. Park, Appl. Phys. Lett. 82 (13) (2003) 2145–2147.
[32] P.T. Moseley, J. Norris, J.O.W. Norris, D.E. Williams, Techniques and Mechanisms in Gas Sensing, Adam Hilger, Bristol, 1991, Chapter 4 and 14.
[33] C. Morterra, M.P. Mentruit, G. Cerrato, Phys. Chem. Chem. Phys. 4 (2002) 676–687.
[34] L. Cao, S.R. Segal, S.L. Suib, X. Tang, S. Satyapaly, J. Catal. 194 (2000) 61–70.
[35] A.A. Tomchenko, G.P. Harmer, B.T. Marquis, Sens. Actuator B-Chem. 108 (2005) 41–55.
[36] A. Ponzoni, C. Baratto, S. Bianchi, E. Comini, M. Ferroni, M. Pardo, M. Vezzoli, A. Vomiero, G. Faglia, G. Sberveglieri, IEEE Sensors J. 8 (2008) 735–742.
[37] C. Yu, Q. Hao, S. Saha, L. Shi, X.Y. Kong, Z.L. Wang, Appl. Phys. Lett. 86 (6) (2005) 063101.